J.Fluid Mech. (1968), *vol.* 34, *part* 1, *pp.* 25–48
Printed in Great Britain

Further experiments on steady separated flows past bluff objects

By ANDREAS ACRIVOS, L. G. LEAL, D. D. SNOWDEN† AND F. PAN‡

Department of Chemical Engineering, Stanford University, California

(Received 17 November 1967)

Detailed experimental results are presented for the steady separated flow past a variety of bluff objects. Included in this work are measurements of: rear stagnation point pressure coefficients; the pressure distribution along the base of a backward-facing step; velocity profiles within the circulating wake-bubble as well as in the outer flow; lengths, maximum widths and vortex centre locations of the corresponding wake-bubbles; and the local shear stress along the surface of a circular cylinder. In every case, the experimental data were found to be consistent with the theoretical model proposed by Acrivos *et al.* (1965) for the steady separated flow past bluff objects in the limit of large Reynolds numbers R.

1. Introduction

The present study is aimed at furthering our understanding of steady separated flows past bluff objects in the limit of high Reynolds number R. In particular it is intended to investigate in some detail a theoretical model recently proposed by Acrivos *et al.* (1965) for the structure of the closed wake, which was based on the following experimental results of Grove *et al.* (1964) for circular cylinders: (i) the pressure coefficient at the rear stagnation point reaches a finite negative value ($\approx -0{\cdot}5$) at $R = 25$ beyond which it remains independent of R; (ii) the length of the closed wake increases linearly with R while its width attains a finite limit of $O(1)$; (iii) the maximum back-flow velocity in the closed wake reaches a limit of $O(1)$ as R is increased. Although the principal steps leading to the formulation of this model have already been described in detail by Acrivos *et al.* (1965), its main features will be summarized here to aid the discussion that follows.

As depicted in figure 1, the closed wake is viewed as consisting of two overlapping flow domains: a relatively stagnant region near the non-wetted surface of the body (designated as I), and the major portion of the wake, of length $O(R)$, where the streamlines are almost parallel (denoted as II). It was shown that, in order to explain the experimental result (i), it is necessary to postulate that the flow within region II must remain viscous everywhere even as $R \to \infty$. This, together with (ii) and (iii), suggested then the transformations $\hat{x} = x/R$, $\hat{v} = vR$,

† Present address: Esso Research and Engineering Co., Florham Park, New Jersey.
‡ Present address: Union Carbide Co., Plastics Division, Bound Brook, New Jersey.

which, when substituted into the Navier–Stokes equations, yielded, for $R \to \infty$,

$$\left.\begin{aligned} u\frac{\partial u}{\partial \hat{x}} + \hat{v}\frac{\partial u}{\partial y} &= -\frac{1}{2}\frac{\partial p}{\partial \hat{x}} + \frac{\partial^2 u}{\partial y^2}, \\ \frac{\partial p}{\partial y} = 0 \quad \text{and} \quad \hat{v} &= -\int_0^y \frac{\partial u}{\partial \hat{x}}\, dy. \end{aligned}\right\} \tag{1}$$

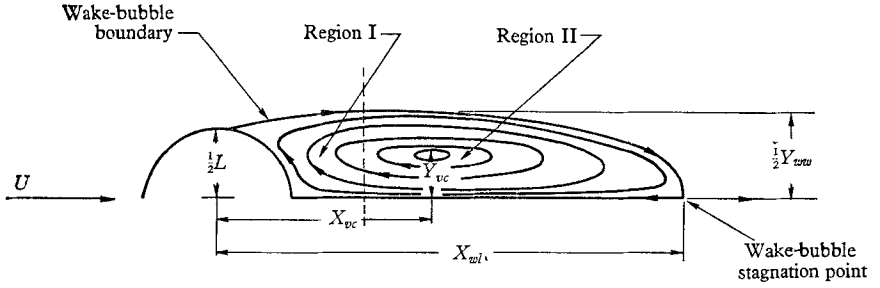

FIGURE 1. Typical wake-bubble.

It was also shown that this system of equations, which contains both viscous and inertia terms, cannot hold within region I since, owing to its parabolic character, it cannot produce a solution satisfying both boundary conditions at the body surface, i.e. the vanishing of u and v; instead, the solution in region II must match with the corresponding solution in region I which satisfies

$$\left.\begin{aligned} \bar{u}\frac{\partial \bar{u}}{\partial x} + \bar{v}\frac{\partial \bar{u}}{\partial y} &= -\frac{1}{2}\frac{\partial \bar{p}}{\partial x} + \nabla^2 \bar{u}, \\ \bar{u}\frac{\partial \bar{v}}{\partial x} + \bar{v}\frac{\partial \bar{v}}{\partial y} &= -\frac{1}{2}\frac{\partial \bar{p}}{\partial y} + \nabla^2 \bar{v}, \end{aligned}\right\} \tag{2}$$

with $\bar{u} = uR$, $\bar{v} = vR$ and $\bar{p} = pR^2$. It should be noted that these equations are now elliptic and contain, once again, both viscous and inertia terms.

This theoretical model for the wake, in addition to being consistent with Grove's results, also leads to the following interesting and, perhaps, surprising predictions for large R: that the wake bubble should be structurally similar in the $(\hat{x}, y)$-plane; that the pressure gradient along the returning streamline should be $O(1/R)$ within region II; and that both the velocity components u and v in the neighbourhood of the body, i.e. within I, should be $O(1/R)$. The latter also implies that the pressure drop across I should be $O(1/R)^2$.

The motivation for the present study arose primarily from two considerations. First, since the theoretical arguments outlined above should apply, in principle, irrespective of the form of the bluff body responsible for the formation of the wake bubble, results analogous to those obtained for the circular cylinder should also be expected from experiments using other bluff objects. And, secondly, for the theoretical model to be valid, its predictions which were listed earlier should also withstand experimental test. This applies particularly to the

second prediction, which, as pointed out in detail by Acrivos *et al.* (1965), is incompatible with any standard potential-flow analysis over the long but slender body representing the solid object plus its associated closed wake, thereby introducing into the theoretical model a possible inconsistency.

Thus Grove's measurements were extended to the following objects: a flat plate placed both normal to the direction of the mainstream as well as at angles 30° and 60°; wedges having vertex angles 30° and 60°; a circular and a half circular cylinder; and, finally, a backward facing step. In addition, velocities were measured behind a vertical flat plate in order to verify the third prediction of the theoretical model, while, to test the second prediction, measurements were made of the pressure variation along the base of the backward-facing step and of the corresponding velocity profile outside the wake-bubble. It will be shown that all the new experimental data are completely consistent with the theoretical model proposed earlier, but that, unfortunately, the possible inconsistency referred to above between our model and the potential flow calculations still could not be resolved.

In what follows, we shall present the principal results of this experimental study.

2. Experimental apparatus and techniques

The experiments were carried out in a closed loop oil tunnel which, as shown in figure 1 of Grove *et al.* (1964), consisted mainly of a centrifugal pump that recirculated the oil at constant flow rates, a test section (figure 2) made of Plexiglas for visual observation, and a refrigeration unit for keeping the oil temperature constant (within 0·2 degC). Ahead of the test section were located a set of screens which served to minimize velocity non-uniformities. Details of the construction as well as the operating features of the tunnel are described by Snowden (1967) and by Grove (1963).

Since the flow field in the tunnel accelerated slightly owing to the formation of boundary layers on the walls, the task of determining the free-stream velocity as well as the static pressure that would exist in an 'equivalent' unbounded domain was a matter of obvious importance. Here we followed Grove *et al.* (1964) by choosing, for the 'free' stream velocity, the centreline fluid velocity at the test piece position under the same operating conditions but without the object, and, as the reference pressure, the pressure on the wall directly underneath the point of measurement. The latter seemed preferable to using a single reference pressure at a fixed point in the tunnel, because the dimensionless reference static pressure on the wall was found to vary by as much as 0·1 along the length of the wake owing to the blocking effect of the object plus its wake. On the other hand, since the acceleration of the velocity field in the empty tunnel over a wake length (3–6 in.) never amounted to more than 3 %, which is within the accuracy of the measurements, it was felt that a single 'free' stream velocity would suffice to normalize all the pressure data. Although somewhat arbitrary, these choices are, at least, entirely consistent with the usual definitions when the test object is small.

As is evident from the work of Grove *et al.* (1964), the blockage of the tunnel by the test object affects quantitatively the experimental results. Hence it was obviously desirable to use test objects as small as was experimentally practicable in order to minimize the blockage ratio L/h† and, therefore, the blockage effect.

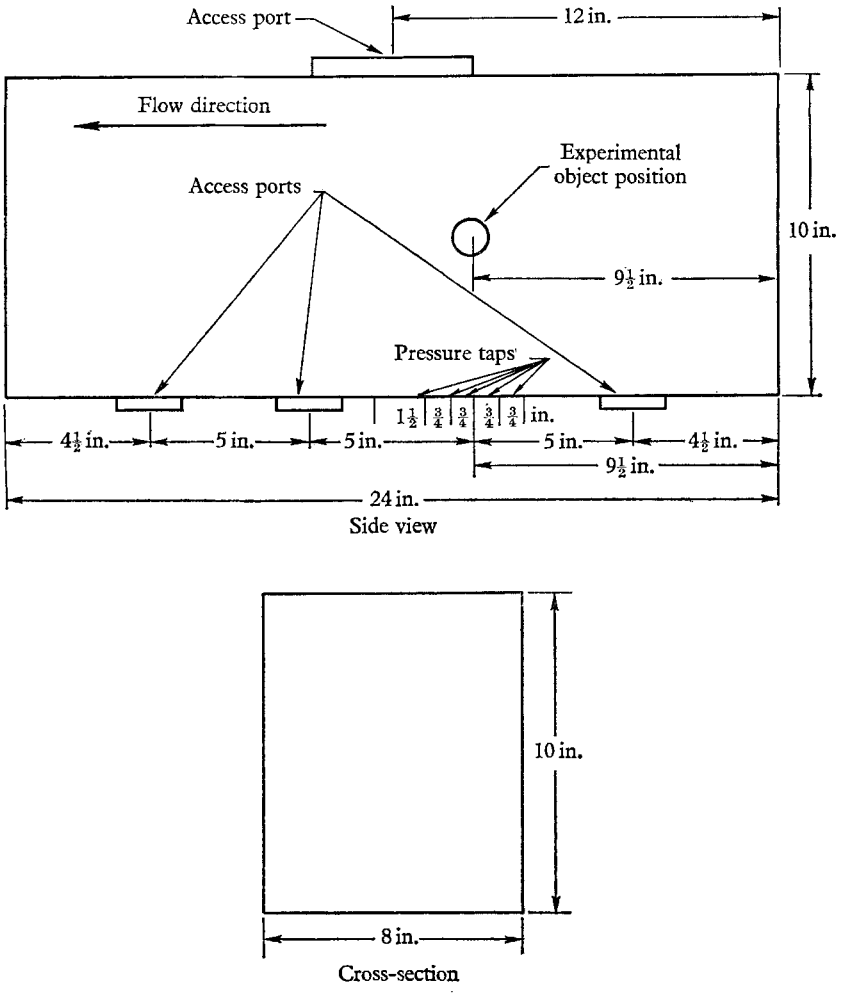

FIGURE 2. The test section.

The compromise appeared to be $L = \frac{1}{2}$ in. ($L/h = 0{\cdot}05$). Although errors introduced by this slight blockage are believed to be small enough so as not to affect in any significant way the measured quantities upon which the model is based, possible inaccuracies caused by this blockage effect will be discussed in some detail later on wherever appropriate.

† L is the characteristic length appearing in the definition of the Reynolds number and is taken to be the diameter for the circular cylinder and half-cylinder, the wedge base height for the 30° and 60° wedges, and the chord length for the flat plate. The distance between the bottom and the top surfaces of the test section is denoted by h, which, in our case, was equal to 10 in.

As also described by Grove *et al.* (1964), a splitter plate was used to stabilize the wake up to Reynolds numbers considerably in excess of those at which instabilities would set in otherwise. To minimize the influence of the plate on the flow structure the splitter plate was positioned as far back as possible while still maintaining a steady wake-bubble, which, experimentally, was found to be such that the front tip of the plate was located at a distance approximately $3L$ from the downstream edge of the object. Even so, the position of the splitter plate relative to the object did exert an influence on the experimental results, but this will be discussed later on in appropriate sections.

Finally, flow visualization was achieved by simply entraining into the tunnel some air which, after a few passes through the fine screens, broke up into a large quantity of tiny bubbles. Since these bubbles were very small, their effect on the flow field was negligible and their vertical velocity due to buoyancy slight; thus their streaks on a photograph exposed for short times gave a proper representation of the streamlines at steady state. These pictures were taken by focusing a large lens with a narrow depth of field (about 5 mm) on the mid-section of the tunnel, which was illuminated from the top by a slit light source in order to improve the contrast between the tracer streaks and the background. A typical streamline pattern of the wake-bubble behind a circular cylinder set normal to the flow is shown in figure 3, plate 1.

3. Results

(*a*) *Wake structure*

A large number of experimental results are reported by Snowden (1967) for the bluff objects listed in table 1. In every case it was found that the wake length, X_{wl}, which is defined as the distance between the base of the bluff body and the wake stagnation point (in the case of the circular cylinder this distance was

	$\hat{p}_{180} = \frac{p_{180} - p_{\text{stat}}}{\frac{1}{2}\rho U^2}$	K	Y_{ww}/L
Circular cylinder (L/h = 0·050)	−0·47	0·064	1·25
Circular cylinder (L/h = 0·025)	−0·43	0·070	1·35
Half cylinder (L/h = 0·050)	−0·52	0·077	1·25
Flat plate (L/h = 0·050)	−0·60	0·097	1·35
Wedge, 30° (L/h = 0·050)	−0·45	0·046	1·20
Wedge, 60° (L/h = 0·050)	−0·55	0·063	1·35

TABLE 1

measured from the axis of the cylinder), increased linearly with Reynolds number, whereas the maximum width, Y_{ww}, of the wake approached a limiting value of $O(1)$. Furthermore, the vortex centre also moved downstream in direct proportion to the Reynolds number. In fact, it was found that, for blockage ratios below 0·1 and for $R > 30$, $Y_{vc}/Y_{ww} \sim \frac{3}{5}$ and $X_{vc}/X_{wl} \sim \frac{1}{3}$ for all the tested objects

including even the circular cylinder, if X_{vc} and X_{wl} were measured from the rear stagnation point. Also, of particular significance was the observation that the streamline patterns within all the wake-bubbles remained qualitatively similar in the $(x/R, y)$-plane and retained the general appearance of the pattern depicted in figure 3. These results are clearly consistent with the Acrivos *et al.* (1965) model which predicts that at high Reynolds numbers the shape and the streamline structure of the wake should be independent of R in the $(x/R, y)$-plane. The proportionality constant, K, between the wake length (in the absence of the splitter plate) and the Reynolds number, for the different objects, as well as the corresponding maximum widths of the closed wakes are tabulated in table 1.

A plot of wake length *vs.* Reynolds number for the cylinder, typical of such results for all the objects listed in table 1, is shown in figure 4, where it is seen clearly that the presence of the splitter plate inhibits to some extent the growth

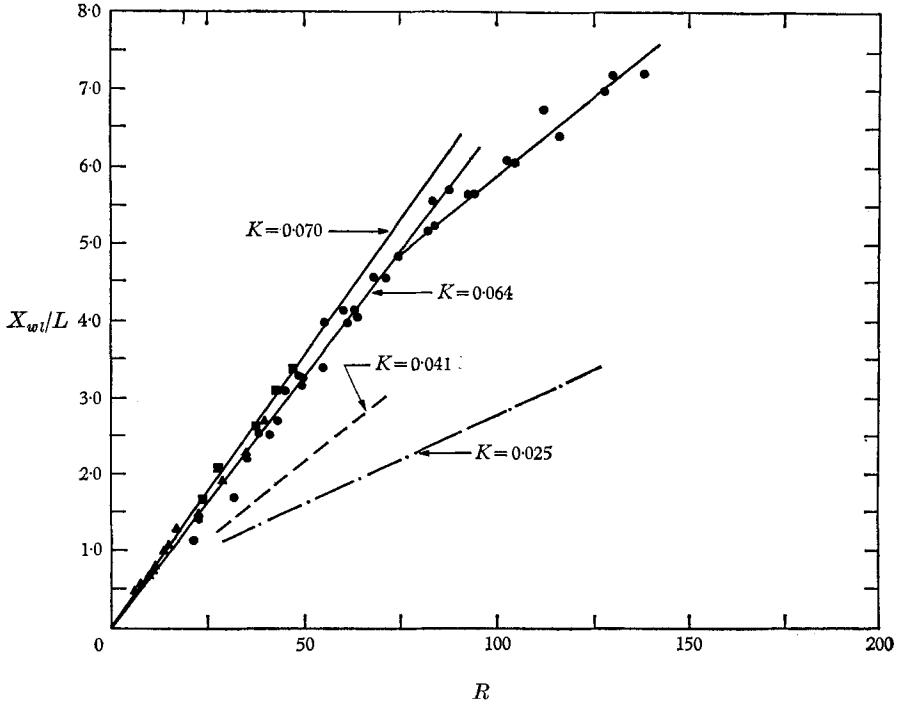

FIGURE 4. The effect of Reynolds number on the wake length of a circular cylinder. Blockage ratio: ■, 0·025 (this work); ●, 0·05 (this work); ▲, 0·03 (Taneda); – – –, 0·10 (Grove); —·—, 0·20 (Grove).

of the wake-bubble. Nevertheless, the experimental data fall along two straight lines, one covering the lower range of Reynolds numbers where no splitter plate is required, and a second through the high Reynolds number points. Thus it should be kept in mind that, although the presence of the splitter plate does lower the value of the proportionality constant, K, it does not seem to affect in any way the conclusion that the wake length is indeed linearly related to the Reynolds num-

ber R. The influence of the tunnel wall on the wake length is also illustrated in figure 4, which shows that the value of K increases with decreasing blockage ratio. However, the fact that our results with $L/h = 0{\cdot}05$ and $L/h = 0{\cdot}025$ are practically identical and also that they agree with those of Taneda (1956), in which $L/h \leqslant 0{\cdot}03$, indicates that, as far as the wake length *vs.* R relation is concerned, the blockage effect in our tunnel was minor for the objects of table 1 if $L \leqslant \frac{1}{2}$ in.

(*b*) *Rear stagnation point pressure coefficient*

A large number of pressure measurements were performed using, first, the manometer technique described by Grove *et al.* (1964) and, later on, a differential pressure transducer recently developed by the Pace Engineering Co. Although in most cases both methods gave comparable results, the transducer was eventually employed exclusively because, owing to its very short response time, data could be obtained with it more rapidly and with better reproducibility than with the manometer.

As in the case of a circular cylinder, for which complete pressure profiles were reported earlier by Grove *et al.* (1964), the pressure coefficient at the rear stagnation point of each of the objects listed in table 1 was found to be substantially negative and to approach a finite and negative limiting value for large R (table 1). Moreover, the dependence of this limiting value of $\hat{p}_{180}$ on the body geometry was found to be qualitatively similar to that predicted by the theoretical model using the approximate technique developed earlier (Acrivos *et al.* 1965) for computing the pressure profile. In fact, it was found that, as the Reynolds number was increased, the pressure coefficient throughout the 'non-wetted' portion of each of the objects became nearly equal to this negative constant appropriate to the given geometry. Although the point at which this rear stagnation pressure coefficient became essentially independent of R varied with the particular object, in all cases this was observed to occur at $R \sim 100$ or before.

In this connexion, it is particularly interesting to observe the pressure variation over the 'non-wetted' perimeter of the flat plate inclined 60° relative to the oncoming stream (figure 5). As one would have expected, the pressure is asymmetric at low Reynolds numbers, but, with increasing R, the pressure at all three pressure taps is seen to approach the same limiting value, which is identical with that on a flat plate placed normal to the stream. In particular, the point at which this occurred ($R \sim 110$) corresponded very closely to the Reynolds number at which obvious asymmetry in the wake-bubble disappeared, thus strongly suggesting that, indeed, at high R, all the wake-bubbles have the same qualitative features irrespective of the shape of the bluff objects, even when the latter is asymmetric.

Finally, since at large Reynolds numbers (> 50) the wake was artificially stabilized by using a splitter plate and since the experiments were performed in a tunnel giving a finite blockage ratio, a number of tests were made to determine the effects of these two factors on the pressure measurements at the rear stagnation point.

As concerns the blockage, it was found that the *front* stagnation pressure coefficient on a $\frac{1}{2}$ in. diameter cylinder ($L/h = 0{\cdot}05$), i.e. the difference between the

stagnation pressure and that at the reference point below the object, approached an asymptotic value of 1·11, whereas the corresponding value for a $\frac{1}{4}$ in. diameter cylinder was 1·05, both results being almost precisely those one would have expected on the basis of a uniform acceleration of the flow field due to the finite

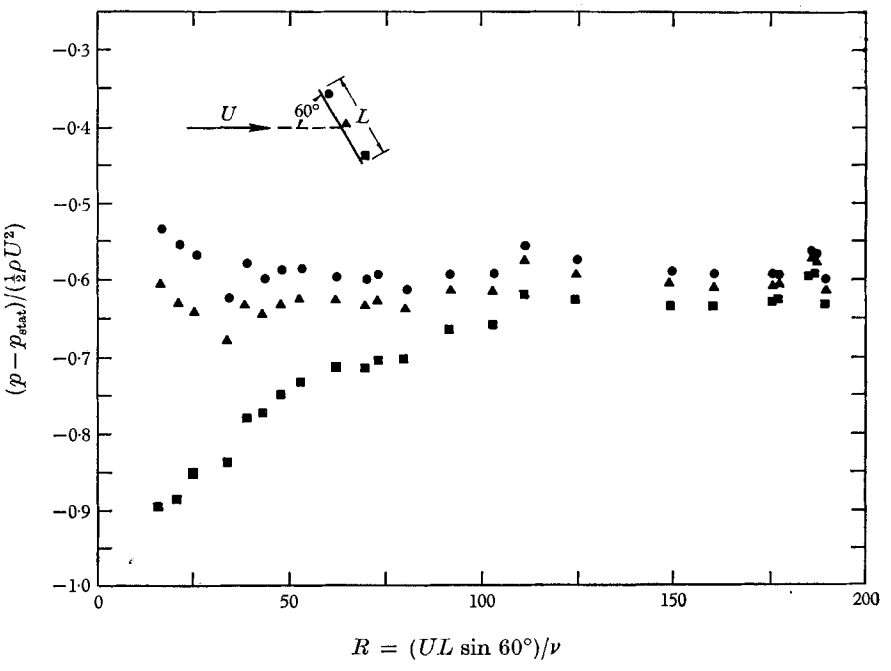

FIGURE 5. The effect of Reynolds number on the pressure profile over the non-wetted surface of a flat plate inclined 60°.

blockage of the object. Similarly, the corresponding *rear* stagnation pressures were, respectively, −0·45 and −0·43 (see figure 6) for $R > 75$, where it should be noted that these refer to the geometrically equivalent cases of the $\frac{1}{2}$ in. cylinder − 4 in. splitter and the $\frac{1}{4}$ in. cylinder − 2 in. splitter. In view of the dependence, described below, of $\hat{p}_{180}$ on splitter plate size, any other choice would have reflected this effect in addition to that of blockage alone. Again, the minor difference between these two values of $\hat{p}_{180}$ is explainable in terms of the overall acceleration of the free stream, and, hence, a non-zero rear pressure coefficient (equal to, approximately, −0·41) should certainly be expected even if $L/h \to 0$.†

Compared to the blockage, the effects of the splitter plate were somewhat more difficult to ascertain in that the measured values of the rear pressure coefficient were found to be dependent on both the position of the plate and, to a minor extent, on its length. On the other hand, the thickness of the splitter plate, in the

† To be sure, the blockage is still seen to affect the stability of the wake in that, as is evident from the data of figure 6 without the splitter plate, the critical Reynolds number for wake instability appears to be around 60 for $L/h = 0{\cdot}05$ rather than 40 as is the case for zero blockage. However, this is to be expected since it was shown in a previous publication (Shair *et al.* 1963) that the stability of the wake is much more strongly dependent on the blockage ratio than are other parameters of the flow around a solid object.

range $0{\cdot}04 <$ thickness$/L < 0{\cdot}07$, had no measurable effect upon the experimental results. Shown in figure 7 are three plots of $\hat{p}_{180}$ *vs.* c/L for the $\frac{1}{2}$ in. ($L/h = 0{\cdot}05$) circular cylinder, c being the distance from the rear stagnation point to the front edge of the splitter plate. It is apparent that the effect of position upon

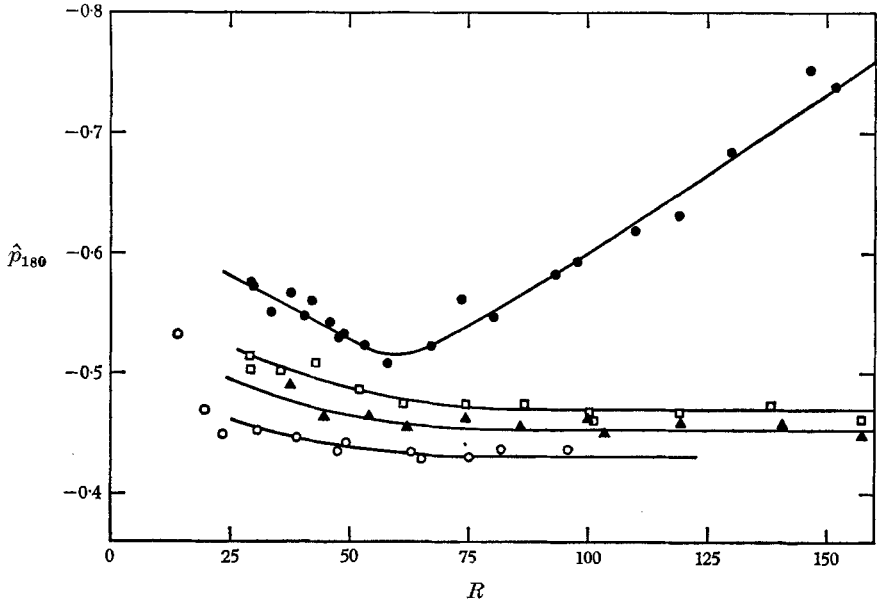

FIGURE 6. The effects of splitter plate size and of blockage on the rear pressure coefficient of a circular cylinder. ●, $\frac{1}{2}$ in. cylinder, no splitter; □, $\frac{1}{2}$ in. cylinder, 2 in. splitter; ▲, $\frac{1}{2}$ in. cylinder, 4 in. splitter; ○, $\frac{1}{4}$ in. cylinder, 2 in. splitter.

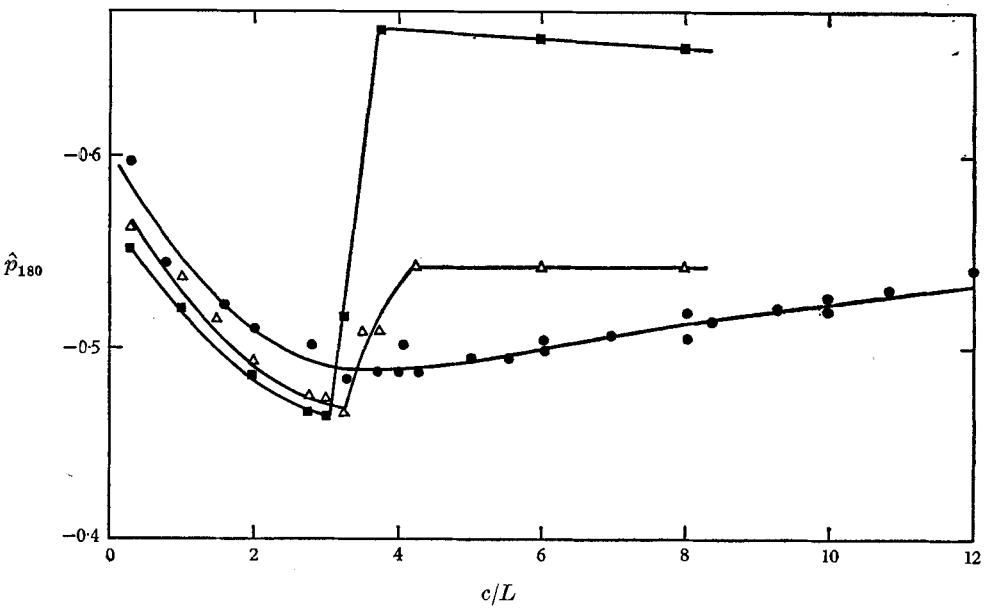

FIGURE 7. The effect of splitter plate position on the rear pressure coefficient for a circular cylinder. ●, $R = 36{\cdot}5$; △, $R = 74{\cdot}5$; ■, $R = 119{\cdot}5$. (Splitter length)$/L = 4{\cdot}0$. $L/h = 0{\cdot}05$.

$\hat{p}_{180}$ was particularly severe at high R where the wake would be unstable if the splitter were absent. Even with the splitter plate present, however, the portion of the wake near the non-wetted surface was found to become unstable when $c/L > \sim 3$. This instability is reflected in the large jump to more negative values of $\hat{p}_{180}$, which can be seen in figure 7. Surprisingly, though, even for $R = 36{\cdot}5$, where the wake appeared to be stable for all splitter plate positions, the value of $\hat{p}_{180}$ was observed to depend on c/L even when the latter was much larger than X_{wl}/L.

In all the other experiments reported here, including those of table 1 and figure 6, the splitter plate was set at $c = 2{\cdot}8L$ since this represented the maximum value of c which ensured a stable wake over the range of R investigated. Moreover, as is evident from figure 7, these results with $c/L = 2{\cdot}8$ represent, in all cases, the least negative values of $\hat{p}_{180}$ attainable with a particular splitter plate arrangement, and hence it seems reasonable that our conclusions concerning the finite negative values of $\hat{p}_{180}$ as $R \to \infty$ could not be influenced by a change in the size of the splitter plate or in its position. Indeed it is significant that the values of $\hat{p}_{180}$ measured in the *absence* of the splitter were always found to be considerably more negative than those measured with the splitter plate present, even for low R where the stability of the wake no longer presented a problem. Although, admittedly, it is not possible to prove conclusively that the steady-state asymptote of the rear coefficient would really approach a non-zero value for splitter positions in excess of $c/L = 2{\cdot}8$ and Reynolds numbers exceeding 50, the approximate critical value for instability, comparison with the stable $R = 36{\cdot}5$ case would seem to indicate that, if anything, the values reported here represent approximate *upper* bounds to the 'true' steady-state rear pressure coefficients at any given R.

(*c*) *Velocity measurements*

Although Grove *et al.* (1964) have already reported that the back flow velocity along the returning stagnation streamline, $-u/U$, reaches a finite limit ($\sim 0{\cdot}22$) which is independent of R, their results were obtained using a 2 in. diameter cylinder which gave a blockage ratio of 0·2. Hence it was felt desirable to repeat their experiments with a $\frac{1}{2}$ in. vertical flat plate ($L/h = 0{\cdot}05$) to make certain that this conclusion was not due somehow to the blockage effect. These experiments were also extended to the portion of the wake close to the plate in order to test the prediction of the theoretical model that the velocity would be $O(1/R)$ in region I. All the velocity measurements were taken using the stroboscopic air-bubble tracer technique (Grove 1963). As shown in figure 8, $-u/U$ was, indeed, independent of the R and nearly constant ($\sim 0{\cdot}17$) over a large portion of the wake, while, at a fixed point near the flat plate ($y = 0$, $x/L = 0{\cdot}5$), the fluid velocity diminished with increasing R (figure 9). Although the apparent linearity of the data for $R > 90$ when plotted against $1/R$ should, perhaps, not be taken at face value owing to the scatter of the data and the limited range of the Reynolds number, the trend towards 'stagnancy' in region I is clearly demonstrated, thus providing strong support for the validity of the theoretical model.

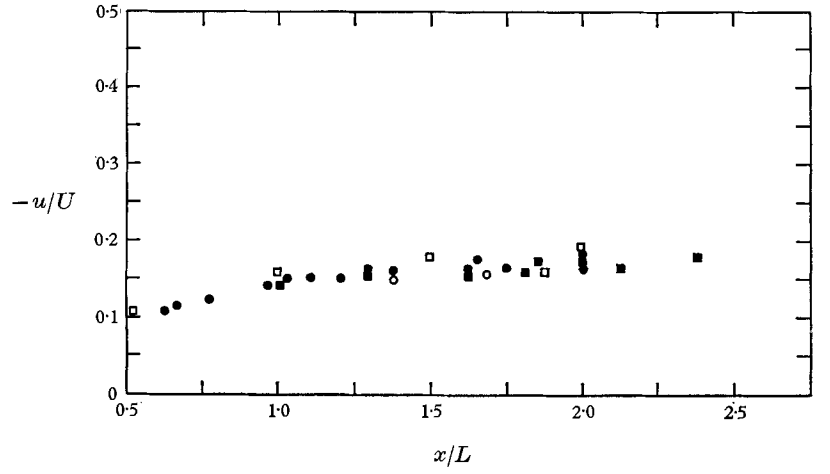

FIGURE 8. The backflow velocity along the returning stagnation streamline of a flat plate normal to flow. $x \equiv$ distance back of flat plate. □, $R = 87$; ●, $R = 103$; ■, $R = 133$; ○, $R = 165$.

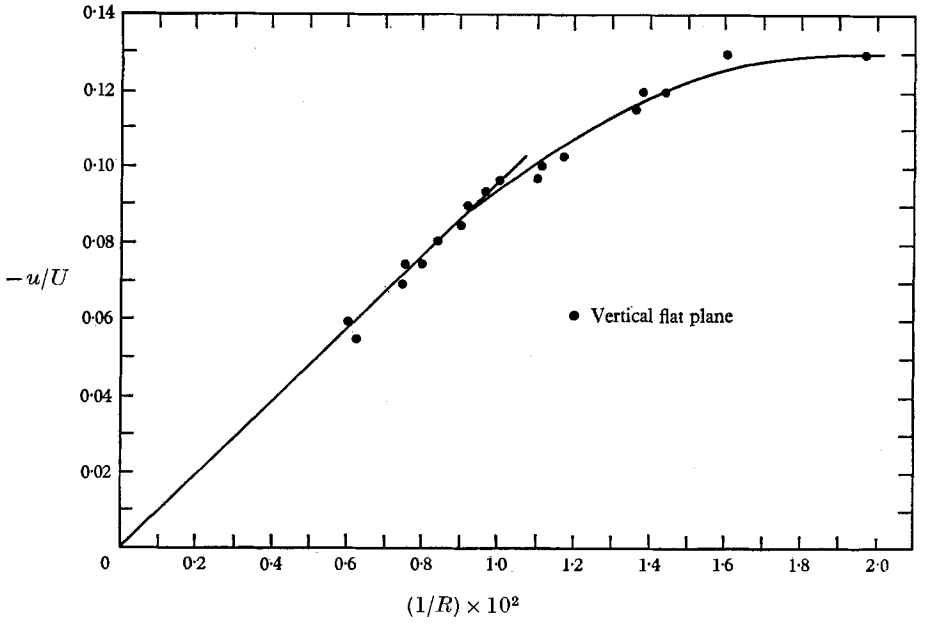

FIGURE 9. The effect of Reynolds number on the velocity along the returning stagnation streamline at $x/L = 0{\cdot}5$.

(*d*) *The shear stress at the surface of a circular cylinder*

In a previous article (Acrivos *et al.* 1965) it was shown that valuable information about the state of motion in the neighbourhood of the cylinder surface could be obtained by measuring the surface temperature of a uniformly heated cylinder. Even more helpful in this connexion is the local shear stress on the surface, which can be measured indirectly using the heated surface probe technique.

The basic principles of this method, which, apparently, was first used by Ludwieg (1950), have been discussed recently by Snowden (1967) and by Rotem (1967). Briefly, it involves measuring the rate of heat transfer to a fluid in motion from a narrow isothermal electrically heated metal strip positioned parallel to the cylinder axis and flush with its surface. Then, if the Prandtl number σ of the fluid is sufficiently large for the thickness of the thermal layer to be small, the usual dimensionless energy equation can be replaced by

$$2\beta y \frac{\partial T}{\partial \theta} - \frac{d\beta}{d\theta} y^2 \frac{\partial T}{\partial y} = \frac{1}{R\sigma} \frac{\partial^2 T}{\partial y^2}, \tag{3}$$

where T is the dimensionless temperature, y is the dimensionless distance from the surface along the r-direction, r and θ are the standard cylindrical polar coordinates, and $\beta(\theta) = (\partial u_\theta/\partial y)_{y=0}$.

Equation (3) admits a similarity solution (Acrivos 1960) according to which the Nusselt number Nu, defined by

$$Nu \equiv \frac{\text{total rate of heat input}}{\text{heated area}} \frac{L}{k\Delta T}$$

with k and ΔT being, respectively, the thermal conductivity of the fluid and the temperature difference between the heated strip and the fluid bulk, is given by

$$Nu = \frac{1}{\Gamma(\frac{4}{3})} \left(\frac{3\sigma R}{4}\right)^{\frac{1}{3}} \frac{\left(\int_{\theta_1}^{\theta_2} \sqrt{\beta}\, d\theta\right)^{\frac{2}{3}}}{\theta_2 - \theta_1}, \tag{4}$$

where $(\theta_2 - \theta_1) \equiv 2b/L$ with b denoting the width of the heated metal strip. Therefore, if b is sufficiently small the variation of β along the strip can be neglected, so that equation (4) reduces to

$$Nu = 0{\cdot}807(\sigma R)^{\frac{1}{3}} (L\beta/b)^{\frac{1}{3}}. \tag{5}$$

On the other hand, near the two stagnation points $\theta = 0$ and $\theta = \pi$ where, owing to symmetry, β equals, respectively, either $B_0\theta$ or $B_1(\theta - \pi)$ with B_0 and B_1 being constants, equation (4) becomes

$$Nu = 0{\cdot}775B^{\frac{1}{3}} (\sigma R)^{\frac{1}{3}} \tag{6}$$

where B is either B_0 or B_1. Thus β and, therefore, the local shear stress at the surface can be obtained directly from equations (5) and (6) once the total heat flux and the temperature on the strip are determined experimentally.

The heated probe consisted of a lucite cylinder $\frac{3}{4}$ in. in diameter which, when installed, completely spanned the test section. A rolled copper strip less than 0·010 in. in thickness and about $\frac{1}{16}$ in. wide (equivalent to $\theta \cong 9$ degrees) was carefully positioned on tiny ledges above a groove cut longitudinally along the cylinder surface. The air space provided by the groove below the copper strip served to insulate the strip and furnished a passage for leads attached to thermocouples soldered to the underside of the strip. The electrical heating for the copper strip was provided by a high current, low voltage, a.c. power supply. Also, the

Prandtl number of the oil was in excess of 1000, thus ensuring the applicability of equation (3). Further details are given by Snowden (1967).

Shown on figure 10 are values of $\beta^* = \beta R^{-\frac{1}{2}}$ along the wetted perimeter of the cylinder which were obtained at Reynolds numbers of 64, 81, 100, 121 and 144,

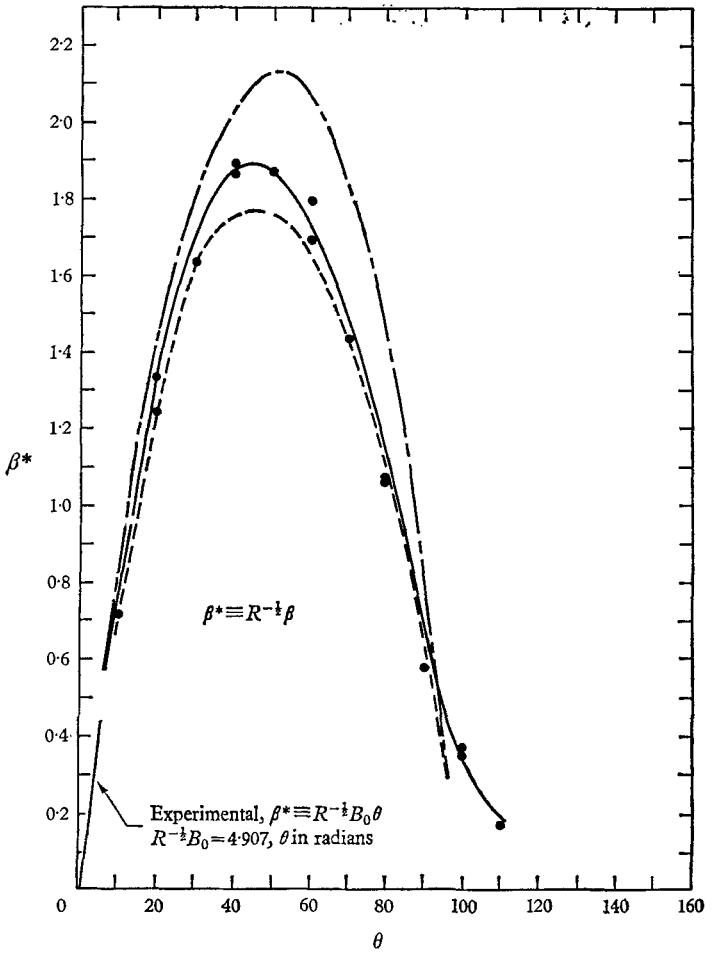

FIGURE 10. The shear stress at the wetted surface of a circular cylinder ($64 \leqslant R \leqslant 150$). —•—, experimental, heat transfer method ($\frac{3}{4}$ in. diameter cylinder); – – –, from pressure distribution ($\frac{1}{2}$ in. diameter cylinder); ———, from pressure distribution (1 in. diameter cylinder).

using the heated surface probe technique just described. Also shown are two theoretical curves computed from an approximate solution of the laminar boundary-layer equations using, as the pressure profile up to the point of detachment, the measured pressure distribution along the cylinder surface reported by Grove *et al.* (1964). It is seen that over the front half of the cylinder the agreement between the curves is excellent, the slight discrepancies being due, in all likelihood, to the blockage effect.

In contrast, as seen in figure 11, the values of β near the rear stagnation point were found to *decrease* with increasing R in accordance with the prediction of the theoretical model and in agreement with the velocity measurements shown in figure 9. A trend similar to that seen in figure 11 was also evidenced all along the non-wetted perimeter of the cylinder (Snowden 1967). Although, again, the apparent linearity of the data when plotted against $1/R$ should not be taken literally, the trend towards 'stagnancy' within region I of the closed wake is, once again, unmistakable.

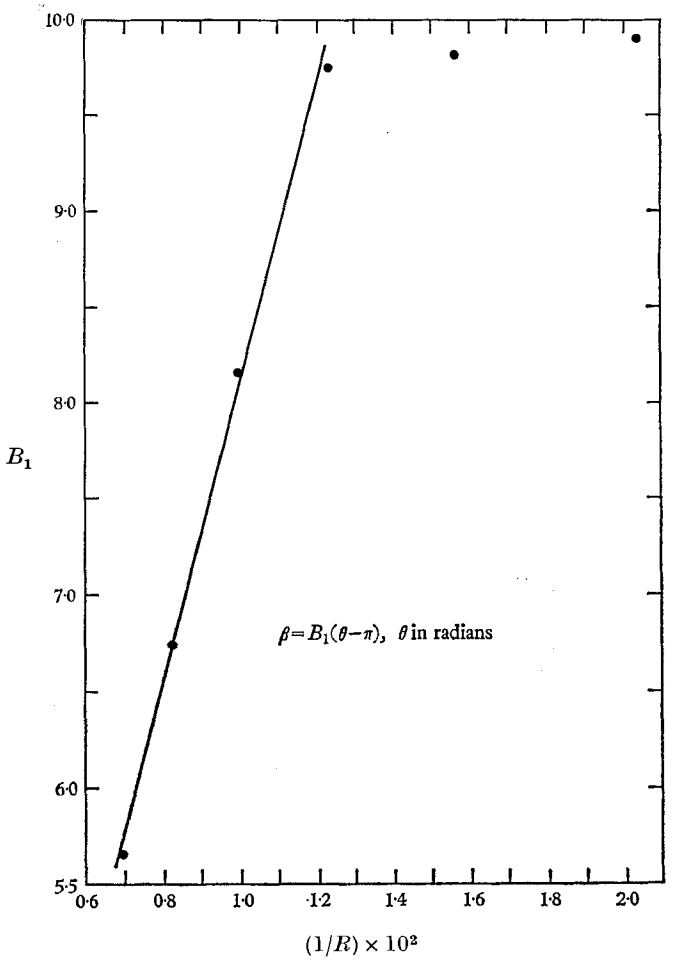

FIGURE 11. The effect of Reynolds number on the shear stress near the rear stagnation point of a circular cylinder.

(*e*) *The backward-facing step*

Compared with the bluff objects studied previously, the backward-facing step (figure 12) enjoys two advantages: first, its use automatically eliminates all questions regarding the possible spurious effects due to the presence of a splitter plate since, now, the 'splitter plate' is an integral part of the system. But,

more importantly, it allows the pressure distribution along the boundary of the closed wake to be inferred by measuring the pressure profile along the base of the step, thus permitting one to test experimentally the prediction of the theoretical model that the pressure gradient along the returning streamline should be

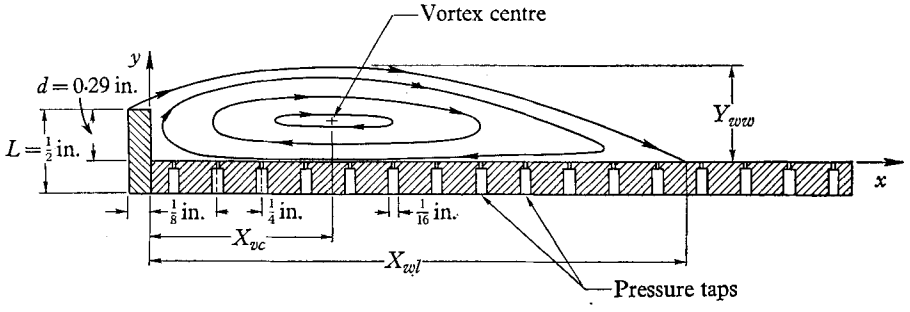

FIGURE 12. The backward-facing step.

$O(1/R)$ within region II of the wake. In all other respects, the backward-facing step is of course very much like all the bluff objects listed in table 1, and hence results for its wake length *vs.* R† relation, for its wake width, etc., should be similar to those obtained earlier.

A typical streamline pattern of the closed wake behind the step is shown in figure 13, plate 1, which depicts the principal features of the wake, such as the separating streamline, the point of reattachment, the vortex centre, etc. As expected, the wake length X_{wl} was found to increase linearly with the Reynolds number (figure 14) but more slowly than for a vertical flat plate without a splitter. The vortex centre also moved downstream in direct proportion to R ($X_{vc}/X_{wl} \sim \frac{1}{3}$, $Y_{vc}/Y_{ww} \sim \frac{2}{3}$, for $R > 30$, both values being independent of blockage for $L/h \leqslant 0{\cdot}05$), and the maximum width of the wake approached a limiting value which, in this case, was approximately twice the depth of the step. These results indicate that the qualitative features of the closed wake behind a step are no different from those behind any other bluff object and are consistent with the requirement of the theoretical model that the asymptotic shape and streamline pattern of the wake be independent of R in the $(x/R, y)$-plane. They are also similar to those of Kawaguti (1965) and Macagno & Hung (1967), who considered the flow through a tube expansion, or its two-dimensional equivalent, in which a circulating region usually exists near the corner if the direction of the flow is from the smaller end to the larger one. Although, admittedly, this case is not entirely analogous to ours since the motion in a tube is constrained in the lateral direction and is basically still of a viscous nature irrespective of the value of R, it is interesting to note, nevertheless, that here too the length of the circulating region was found to increase linearly with R.

In one respect, however, the backward-facing step is inferior to most bluff objects in that, owing to the presence of the solid base all along the returning

† Here, $R = Ud/\nu$ where d, the characteristic length, is the depth of the step (see figure 12).

streamline, its wake is substantially wider ($Y_{ww} \sim 2{\cdot}0$ for a blockage of 0·025 and $\sim 1{\cdot}8$ for a blockage of 0·05) than, say, the wake of an analogous vertical flat plate. Hence, one would expect the corresponding blockage effect to be more pronounced. This, in fact, is seen clearly in figure 14, where it is apparent that the

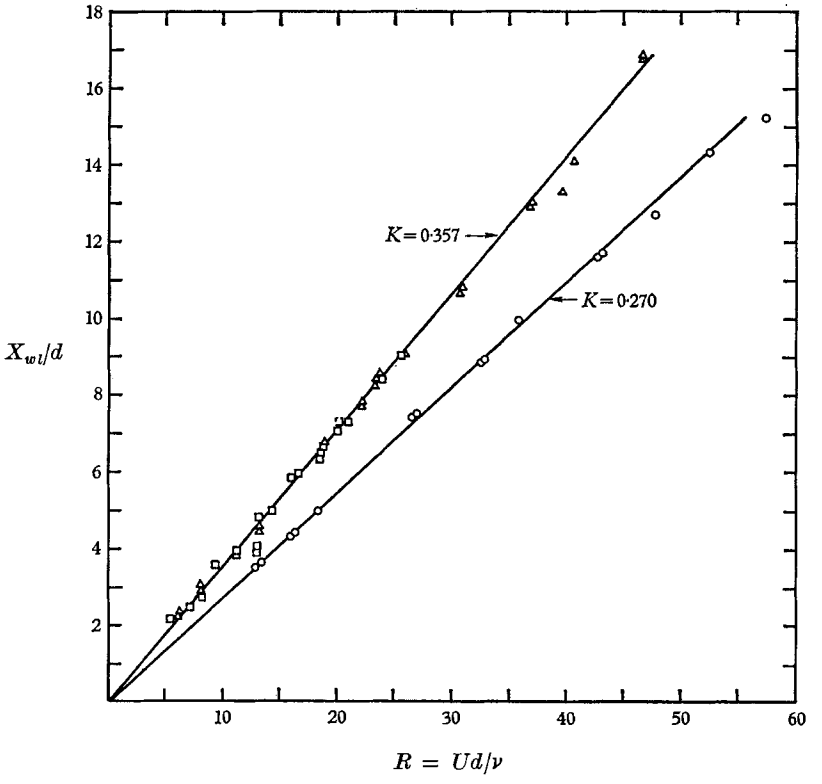

FIGURE 14. The effect of Reynolds number on the wake length, backward-facing step. ○, $L/h = 0{\cdot}05$; △, $L/h = 0{\cdot}025$; □, $L/h = 0{\cdot}0125$.

slope of the wake length *vs.* R line becomes independent of the blockage ratio (L/h) only when the latter is below, approximately, 0·025, in contrast to the previous results (figure 4), where this levelling-off occurred at a blockage ratio approximately twice as large. Unfortunately, it was not found possible to obtain pressure measurements with a step having a depth smaller than about $\frac{1}{4}$ in. (giving a blockage ratio approximately equal to 0·05), and, thus, it should be kept in mind that the data to be reported presently may still be subject to inaccuracies somewhat larger than those for the corresponding measurements given earlier.

The pressure coefficient along the base of the plate is seen plotted in figure 15 for three different values of R. It can be seen that the pressure coefficient at the corner remains finite ($\sim -0{\cdot}63$) and nearly independent of R and that the pressure gradient is almost constant along the major portion of the wake-bubble. In fact, the three sets of data in figure 15, if plotted against the (x/R)-co-ordinate, collapse into a single curve (figure 16) as required by the model of Acrivos *et al.*

In addition, velocity profiles were measured over large portions of the (x, y)-

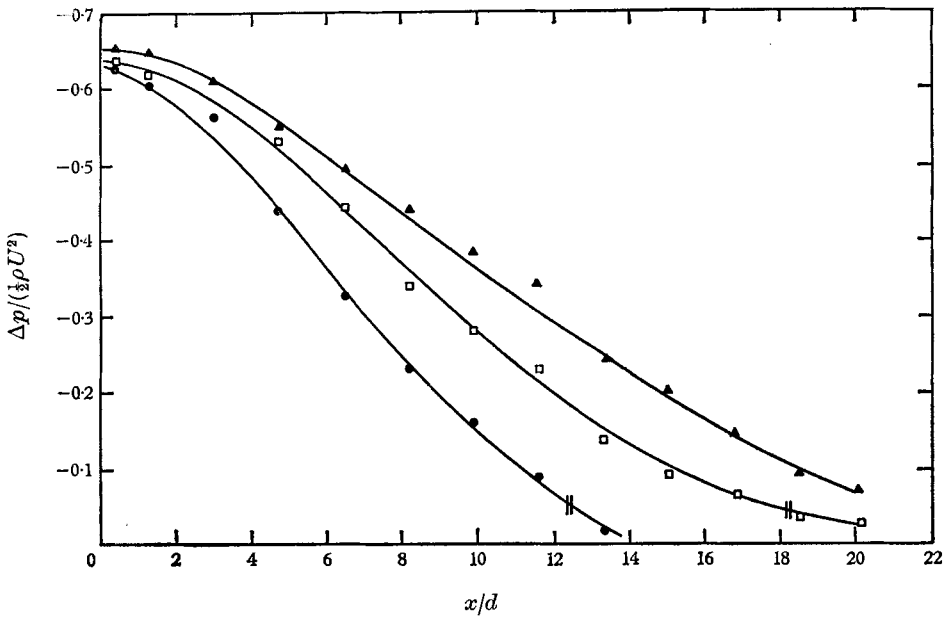

FIGURE 15. The pressure coefficient variations along the returning streamline in the wake. ▲, $R = 81$; □, $R = 61{\cdot}9$; ●, $R = 42{\cdot}5$. || denotes location of wake stagnation point.

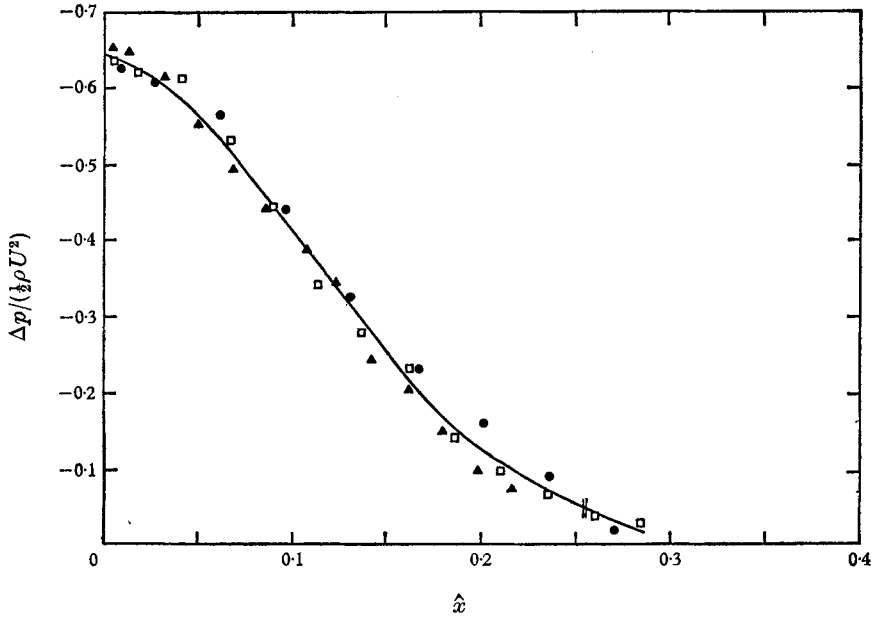

FIGURE 16. The pressure coefficient variations in the stretched co-ordinate $\hat{x}$. ●, $R = 81$; □, $R = 61{\cdot}9$; ▲, $R = 42{\cdot}5$. || denotes location of wake stagnation point.

centreplane of the test section in the presence of a $\frac{1}{4}$ in. step consisting of a $\frac{1}{2}$ in. vertical flat plate ($L/h = 0{\cdot}05$) and a long splitter (length $> X_{wl}$) which touched the non-wetted surface of the plate at its vertical centreline. In accord with the model of Acrivos *et al.*, these profiles were found to reduce to a single plot in the $(\hat{x}, y)$-co-ordinate system when normalized with the corresponding local velocities in the empty tunnel. A typical profile is seen in figure 17 together with the corresponding profile in the empty tunnel, whereas shown in figure 18 is a composite picture of the normalized velocity field near the object. Clearly, the overall acceleration of the flow far from the object relative to that in the empty tunnel (about 10 %) is exactly what one would have expected on the basis of a blockage effect if one were to take into account the width of the wake ($Y_{ww} \sim 1{\cdot}8$).

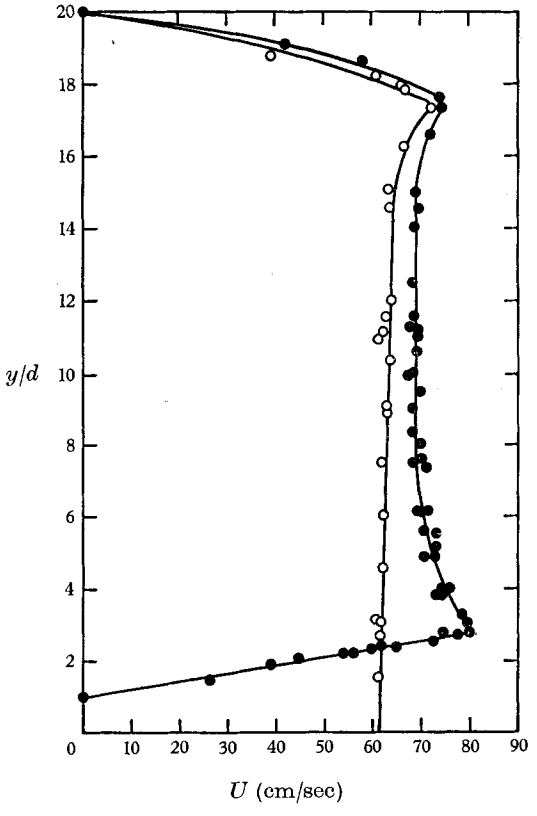

FIGURE 17. A typical experimental velocity profile along the centerplane: ○, in the empty tunnel; ●, in the presence of a step with $L/h = 0{\cdot}05$. $R = 70{\cdot}8$; $\hat{x} = 0{\cdot}05$.

Shown also in figure 18 are the points of maximum relative velocity, which, again, fall on a single curve in the $(\hat{x}, y)$-plane. Of course, because of the negligibly small pressure drop across the wake and its surrounding viscous layer, one would expect these maximum velocities and the corresponding pressures along the base of the step to obey Bernouilli's equation at large R, and indeed, as seen from figures 16 and 18, these two sets of measurements appear to be qualitatively consistent with this last requirement. Unfortunately, however, a quantitative

check could not be devised, owing to the fact that the absolute pressure at any given point within the tunnel could not be maintained at a truly constant value because of unavoidable small variations in the oil level and temperature (i.e. the background pressure).

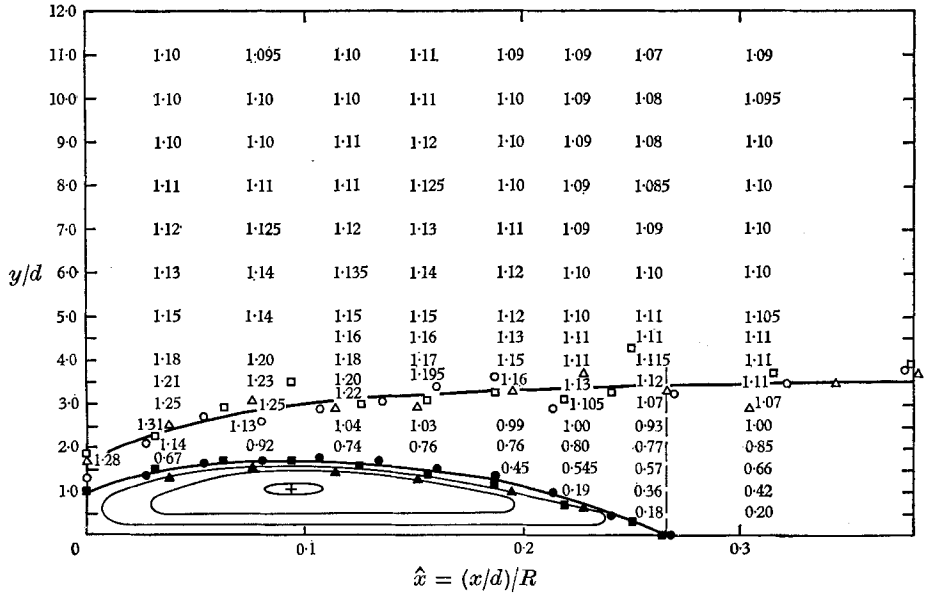

FIGURE 18. Composite velocity profiles and wake-bubble geometry for the backward-facing step with $L/h = 0{\cdot}05$: ○, △, □, position of maximum relative velocity; ●, ▲, ■, position of dividing streamline. ○, $R = 70{\cdot}6$; □, $R = 50{\cdot}8$; △, $R = 36{\cdot}7$.

The step may also be viewed as the limit of the shallow cavity sketched in figure 19. Here, intuitively, one would expect a wake structure similar to that described before as long as the closed wake remained much shorter than the distance between the two vertical sides; but, if the wake were to lengthen and eventually to cover the entire cavity, then one would expect the large R flow in

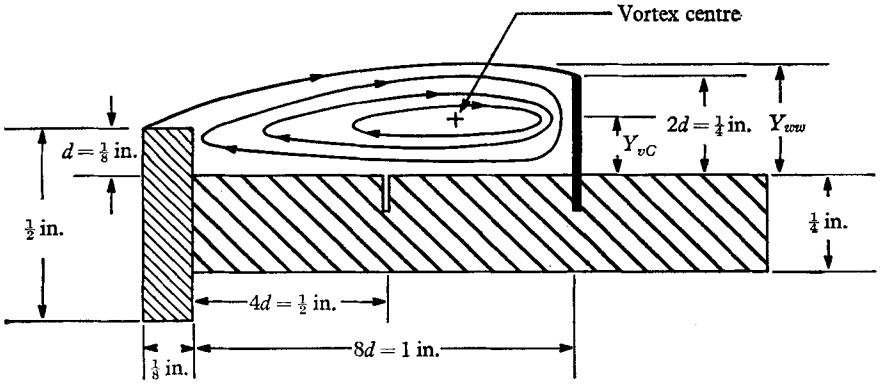

FIGURE 19. The confined cavity.

the region between the two plates to consist of an inviscid uniform vorticity core plus the usual shear layers along the boundaries (Batchelor 1956; Pan & Acrivos 1967).

This interesting transition from a flow having a viscous nature to one becoming inviscid in character is most clearly illustrated, as explained below, in figure 20, where the quantity Y_{vc}/Y_{ww} (defined in figure 19) is plotted against R for wakes constrained at 4- and 8-step heights downstream. Also shown in figure 20 are the corresponding values of Y_{vc}/Y_{ww} over the same range of R for the unconstrained wake behind a step.

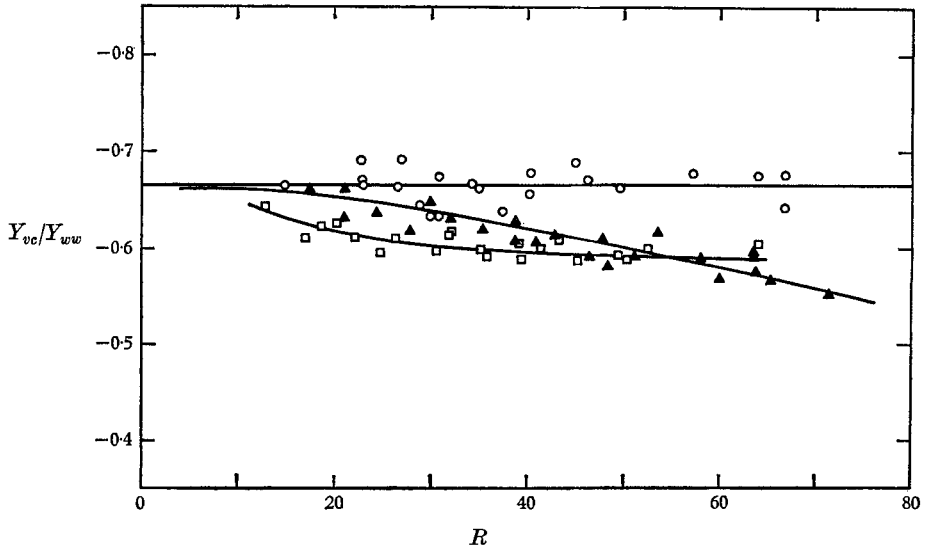

FIGURE 20. The vertical position of the vortex centre in the confined cavity. □, 4/1 cavity; ▲, 8/1 cavity; ○, unobstructed wake.

It is quite easy to show now that, for a wake-bubble having essentially parallel streamlines and obeying (1) with constant $dp/d\hat{x}$ in accordance with figure 16, Y_{vc}/Y_{ww} should be equal to $\frac{2}{3}$, a prediction clearly in excellent agreement with the experimental results of figure 20 for the unconfined wake. Similarly, in a confined wake with parallel streamlines, one would expect Y_{vc}/Y_{ww} to approach $\frac{2}{3}$ as $R \to 0$ and $\frac{1}{2}$ as $R \to \infty$ (Pan & Acrivos 1967), a trend which is evident in the data of figure 20, although only in a qualitative sense.

It is believed that the lack of better agreement is due to the fact that, especially in the case of the 4/1 cavity for which a typical streamline pattern is seen in figure 21, plate 2, the experimentally observed cavities did not consist of the essentially parallel streamlines as envisaged in the above theoretical argument. Indeed, the natural asymmetry was accentuated by the necessity of making the downstream vertical wall nearly twice as high as the original step in order to eliminate the tendency of the system to merely produce a single distorted wake in which, as shown in figure 22, plate 2, the reverse flow climbed over the downstream obstruction. Thus, in order to verify that the observed behaviour truly

corresponded to a transition from a viscous to an inviscid flow, the two limiting cases ($R = 0$, $R = \infty$) were solved numerically for a domain whose shape represented an idealization of that observed experimentally.

In order to simplify the numerical procedure, the shape of the cavity was chosen to consist of a partial wedge with all its boundaries along appropriate co-ordinate lines of a cylindrical polar system. The length-to-height scale based on the smaller of the two 'vertical' surfaces was 4–1 and the numerical scheme involved a simple finite-difference approximation using a 10×20 point mesh. The results of solving numerically

$$\nabla^4\psi = 0, \quad \nabla\psi = 0 \quad \text{on all boundaries except at} \quad \theta = \pi/12{\cdot}5, \quad \text{where}$$
$$\psi = 0, \quad \partial\psi/\partial\theta = 1,$$

$$\nabla^2\psi = -1, \quad \psi = 0 \quad \text{on all boundaries},$$

corresponding, respectively, to the viscous and inviscid limits of the full equations, are seen plotted in figures 23 and 24, from which it is apparent that the

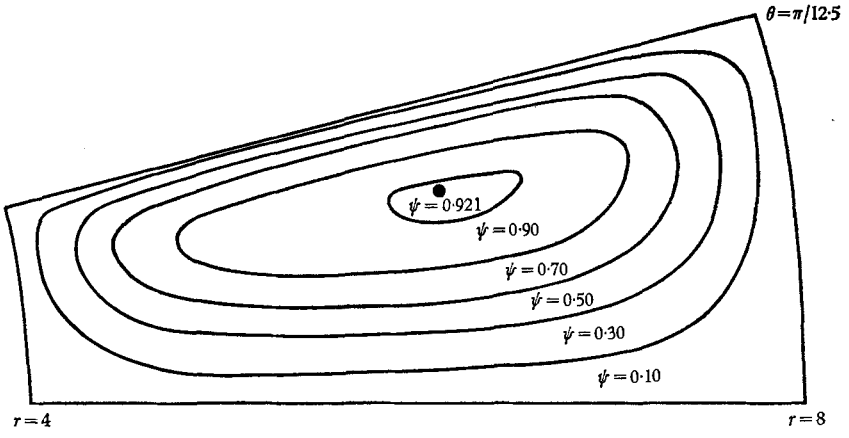

FIGURE 23. Streamline patterns in a confined cavity at $R = 0$ (numerical calculations).

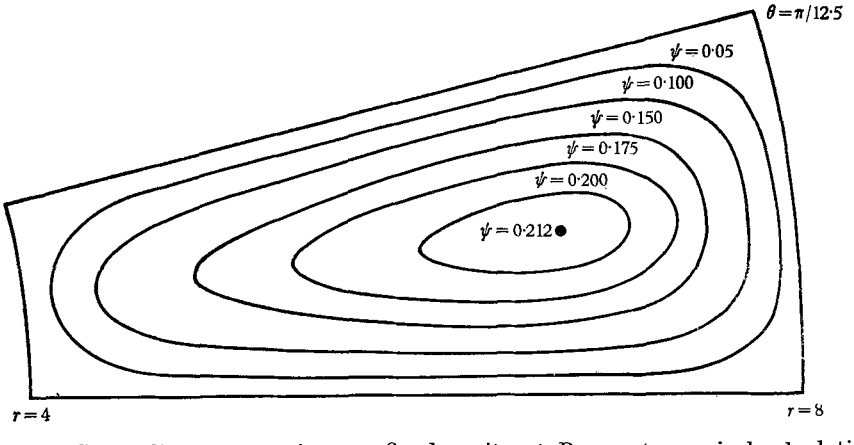

FIGURE 24. Streamline patterns in a confined cavity at $R = \infty$ (numerical calculations).

vortex centre shifts downward and toward the downstream wall as the flow becomes inviscid. Although of course the crude approximation of the cavity shape precludes any quantitative comparisons, these results are in good qualitative agreement with the experiments, where it was observed that the vortex centre not only moved 'down' towards the base, as already indicated in figure 20, but also downstream in the manner suggested by the numerical calculations. Thus, the results are believed to be indicative of a partial transition from a viscous to an inviscid flow in the constrained case over the *same* range of R for which the unconstrained wake was found to remain strictly viscous in nature.

4. Conclusions

A large number of experimental results have been presented for the purpose of testing a recently proposed theoretical model (Acrivos *et al.* 1965) for the steady separated flow past bluff objects in the limit of high Reynolds numbers R. In all respects, the model was found to be consistent with the experimental data. For example, with increasing R, the rear stagnation point pressure coefficients were found to approach a negative value (of order $-\frac{1}{2}$) for a variety of bluff objects, the corresponding wake lengths and widths were shown to be, respectively, $O(R)$ and $O(1)$, and the streamline structure within the various wake-bubbles was observed to remain qualitatively similar in the $(x/R, y)$-plane. Great care was taken to ensure that these results were indicative of the true nature of the steady flow at high R and not due, somehow, to the presence of the stabilizing splitter plate or to a wall effect. Also the prediction of the model that the wake close to the object should become increasingly stagnant relative to the mainstream as $R \to \infty$ was verified experimentally both by means of direct velocity measurements as well as indirectly using a heated surface probe technique.

Particularly significant are the experiments with the backward-facing step which depict the pressure variation along the circulating wake. Once again, there is agreement with the theoretical model in that, as shown in figure 16, dp/dx is $O(1/R)$ throughout the major portion of the wake. Also of significance are the experiments with the shallow cavity showing the change in the vortex centre location with increasing R, for these seem to indicate that a value of R equal to, say, 70 is indeed large enough to bring out any inviscid trends within the flow field in spite of the slow motion inside the cavity relative to that of the mainstream. Thus, it is felt that, within the Reynolds number range of the experiments, a similar trend towards an inviscid flow pattern would have become apparent inside an *unconstrained* wake if such a trend did, in fact, exist.

In conclusion then we have presented a considerable amount of experimental evidence in support of the theoretical model of Acrivos *et al.*, and have shown that the model and its resulting theoretical predictions concerning the nature of the steady flow at large R are everywhere consistent with the experimental measurements. This is in contrast to all previous theoretical models (discussed in detail by Acrivos *et al.*), whose basic features are in fundamental disagreement with our experimental results, provided of course one is willing to grant that the latter are indicative of the true state of steady motion as $R \to \infty$. This also applies to a

recently proposed asymptotic model by Sychev (1967), the main characteristics of which are as follows: a finite drag, a wake-bubble length $O(R)$, a wake-bubble width $O(R^{\frac{1}{2}})$, a rear pressure coefficient $\hat{p}_{180} \to 0$, a wake-bubble becoming *everywhere* stagnant relative to the mainstream, a pressure gradient along the wake-bubble boundary $O(1/R^2)$, and finally a vortex centre location that, in the limit $R \to \infty$, approaches the wake stagnation point, i.e. $X_{vc}/X_{wl} \to 1$. Clearly, except for its first two features, Sychev's model is at variance with our experimental results not only with respect to such measured quantities as $\hat{p}_{180}$ or the wake-bubble width, but also with respect to even such a gross feature of the flow as the predicted streamline pattern within the closed bubble. In fact, it is easy to see that, if all the streamlines within this closed region were to emanate from the wake stagnation point, then the resulting flow pattern would bear practically no resemblance to that which was observed throughout our work (cf. figures 3 and 13) irrespective of the surface geometry, the blockage ratio or the value of R.

To be sure, our model is still incomplete in its present form because it does not explain how it is possible for the external flow to impress a pressure profile similar to that shown in figure 16, along the circulating wake. Indeed, as discussed in detail by Acrivos *et al.* (1965), a straightforward potential flow analysis around any reasonable 'equivalent' body comprising the closed wake and its associated boundary-layer displacement thickness, would lead to pressure profiles in serious disagreement not only with those required by the model but also those measured experimentally in this work. This would imply in turn that such a potential analysis, although proper as $R \to \infty$ for objects of *finite* length, does in fact fail, for reasons that are far from clear at present, when the length of the object is $O(R)$ and its width is still kept $O(1)$.

Thus in this connexion we continue to face a paradoxical and therefore highly intriguing question which strongly demands resolution.

This work was supported in part by grants from the National Science Foundation and the Petroleum Research Fund administered by the American Chemical Society.

REFERENCES

Acrivos, A. 1960 Solution of the laminar boundary layer energy equation at high Prandtl numbers. *Phys. Fluids*, **3**, 657.

Acrivos, A., Snowden, D. D., Grove, A. S. & Peterson, E. E. 1965 The steady separated flow past a circular cylinder at large Reynolds numbers. *J. Fluid Mech.* **21**, 737.

Batchelor, G. K. 1956 On steady laminar flow with closed streamlines at large Reynolds number. *J. Fluid Mech.* **1**, 177.

Grove, A. S. 1963 An investigation into the nature of steady separated flows at large Reynolds numbers. Ph.D. Thesis, University of California, Berkeley.

Grove, A. S., Shair, F. H., Petersen, E. E. & Acrivos, A. 1964 An experimental investigation of the steady separated flow past a circular cylinder. *J. Fluid Mech.* **19**, 60.

Kawaguti, M. 1965 Numerical solutions of Navier–Stokes equations for the flow in a channel with a step. *Madison Research Center Tech. Rept.* no. 574.

Ludwieg, H. 1950 Instruments for measuring the wall shearing stress of turbulent boundary layers. *NACA TM* no. 1284.

MACAGNO, E. O. & HUNG, T. K. 1967 Computational and experimental study of a captive annular eddy. *J. Fluid Mech.* **28**, 43.

PAN, F. & ACRIVOS, A. 1967 Steady flows in rectangular cavities. *J. Fluid Mech.* **28**, 643.

ROTEM, Z. 1967 The heated surface probe for measuring shear stress at the wall in laminar boundary layers. *Canad. J. Chem. Engng.* **45**, 175.

SHAIR, F. H., GROVE, A. S., PETERSEN, E. E. & ACRIVOS, A. 1963 The effect of confining walls on the stability of the steady wake behind a circular cylinder. *J. Fluid Mech.* **17**, 546.

SNOWDEN, D. D. 1967 The steady separated flow past bluff objects. Ph.D. Thesis, Stanford University.

SYCHEV, V. V. 1967 *On Laminar Fluid Flow Behind a Blunt Body at High Reynolds Number*. Report to the Symposium on recent problems in the mechanics of liquid and gases at Tarda, Poland, 18–23 September.

TANEDA, S. 1956 Experimental investigation of the wakes behind cylinders and plates at low Reynolds numbers. *J. Phys. Soc. Japan*, **11**, 302.

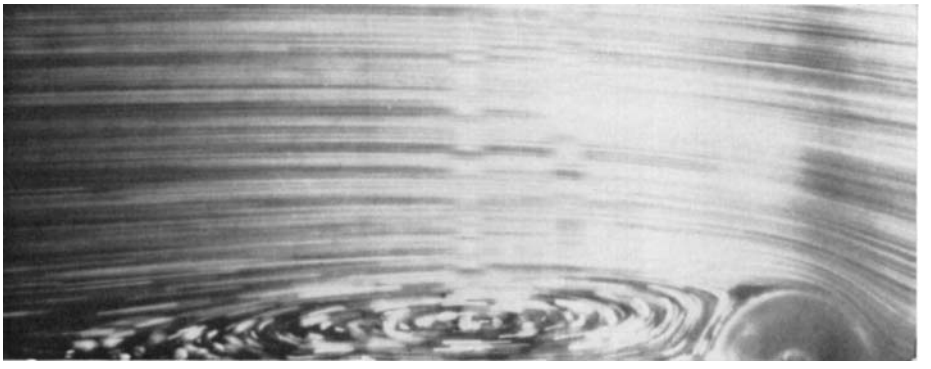

FIGURE 3. A typical streamline pattern for flow past a circular cylinder in the presence of a splitter plate ($R = 75$).

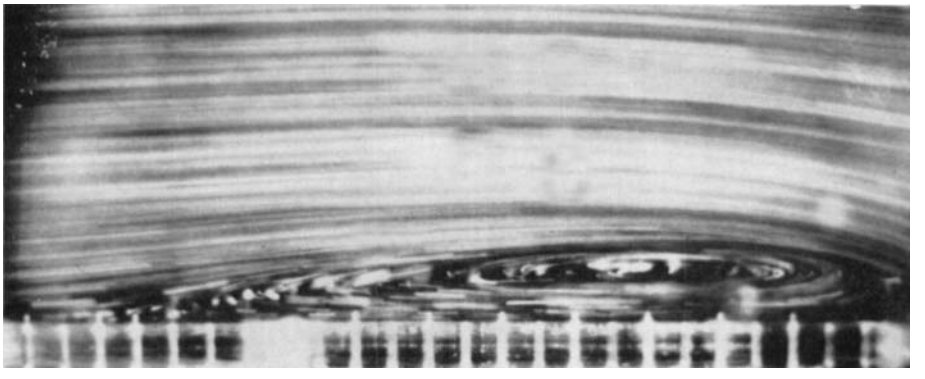

FIGURE 13. A typical streamline pattern for flow past the backward-facing step ($R = 70$; vertical lines in base are the centreplane pressure taps).

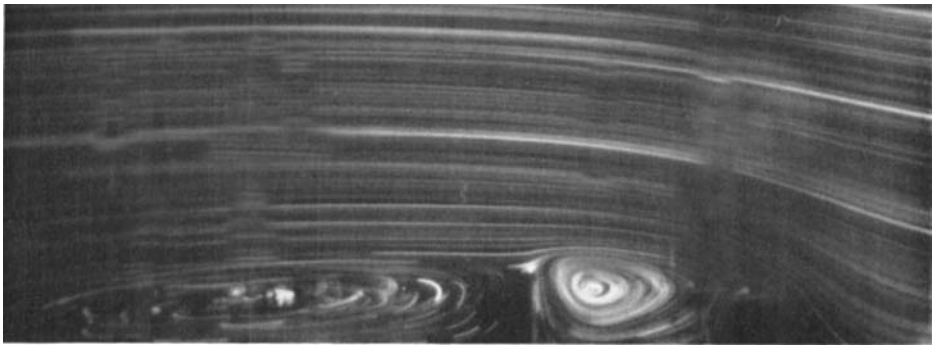

FIGURE 21. Confined cavity of aspect ratio 4/1 at $R = 50$.

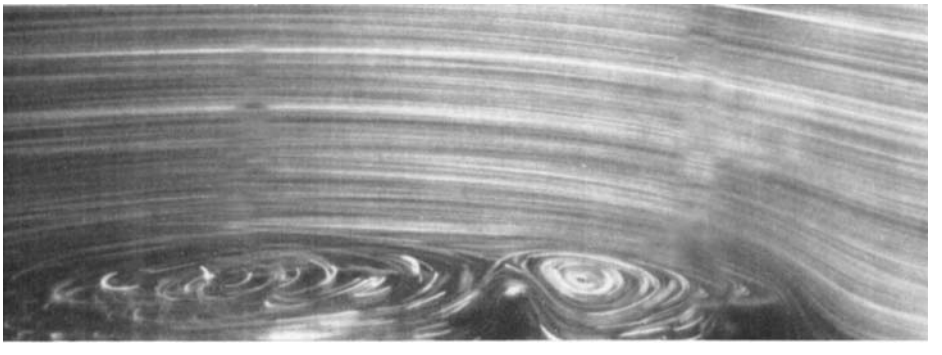

FIGURE 22. Distorted flow in a confined cavity in which the downstream vertical wall is approximately equal to the step height d (aspect ratio 4/1, $R = 50$).